Dalton Transactions

Cite this: *Dalton Trans.*, 2012, **41**, 13364

www.rsc.org/dalton

PAPER

Synthesis, characterisation and adsorption properties of a porous copper(II) 3D coordination polymer exhibiting strong binding enthalpy and adsorption capacity for carbon dioxide†

Pierre Eckold,[a] William J. Gee,[b] Matthew R. Hill*[c] and Stuart R. Batten*[b]

Received 26th June 2012, Accepted 29th August 2012
DOI: 10.1039/c2dt31361h

The synthesis and characterisation of microporous coordination polymers containing copper(II) or cobalt(II) and 2-(pyridin-4-yl)malonaldehyde (**Hpma**) is described and the gas adsorption properties evaluated. Single-crystal X-ray structure determinations identified the structures as $^{3}_{\infty}$[M(**pma**)$_2$]·2X (M = Cu, **1**; Co, **2**; X = MeOH, MeCN), which contain 3D networks with rutile topology and continuous 1D rectangular channels with diameters ranging from 3 to 4 Å. The materials exhibit low BET surface areas of 143 m^2 g^{-1}, but possess large capacities for carbon dioxide capture of 14.1 wt%. The small pore channels are shown to account for this, delivering a particularly strong binding enthalpy to adsorbed CO_2 of 38 kJ mol^{-1}, and a very large adsorption capacity relative to the low surface area.

Introduction

Gas sorption has risen to prominence in recent years due to the pressing need for solutions to mobile storage of alternative fuels such as hydrogen[1] or methane,[2] and the environmental importance of capturing carbon dioxide. The use of adsorbents has opened the possibility of high volumetric and gravimetric capacities at low operating pressures for these applications. In particular, the development of highly-porous coordination polymers (CPs)[3] has been especially significant, given their high surface areas and periodic porosity, which satisfy the stipulated performance criteria[4] for widespread application of these materials.[2,5]

Whilst there is a clear relationship between CP surface area and overall capacity, lower surface area materials that can adsorb large quantities of gas are of interest in more applied settings due to the relative ease with which solvent of synthesis can be removed to activate the sample – many highly porous materials degrade upon activation, or need to be handled in a very sensitive fashion once solvent is removed. More robust materials may deliver simpler handling procedures.

Surprisingly few coordination polymers are known containing pyridine-bearing diketonate ligands, although square grids,[6,7] double chains[7] and heterobimetallic square patterns[8] have been reported using the 3-(4-pyridyl)-acetylacetonato ligand. Furthermore, dialdehyde 2-(pyridin-4-yl)malonaldehyde (**Hpma**) has, with one exception,[9] been utilised solely as an intermediate in the synthesis of ligands, such as pyrazolylpyridine species. The exception, a square-grid network of **Hpma** linking by cobalt nitrate, was obtained by simple mixing of ligand and metal salt in methanol.[9] Therein the ligand was η^2 coordinating *via* both oxygens of the dialdehyde enolate with further coordination blocked by pyridinium formation. The zwitterionic nature of **Hpma** results in atypical structural characteristics, such as the prevalence of the rarely seen *trans*-enolic conformer of a 1,3-dicarbonyl system.[10] Later, it was established using X-ray crystallography that the zwitterionic character of the ligand persists in the absence of a metal centre in the solid state.[11] The unusual stability of the *trans*-enolic conformer can be attributed to the steric freedom allowed by a dialdehyde system relative to other 1,3-dicarbonyl systems (*i.e.* 1,3-diketones), coupled with the conversion of a stabilised intramolecular hydrogen bonding interaction into a mesomeric anionic repulsive force.

Herein we report the formation of new coordination polymers that utilise the unusual *trans*-enolic conformation of the deprotonated dialdehyde **pma** to yield porous materials and investigate their potential gas storage properties. Three microporous coordination polymers were identified by X-ray crystallography as $^{3}_{\infty}$[M(**pma**)$_2$]·2X (M = Cu, X = MeOH (**1a**), MeCN (**1b**); Co, X = MeOH (**2**)). Each was found to contain continuous 1D rectangular channels with a diameter ranging from 3 to 4 Å within the crystalline material and calculated pore volumes of approximately 34%. Other characterisation methods undertaken include thermogravimetric analysis (TGA), elemental analyses and

[a]*Universität Leipzig, Fakultät für Chemie und Mineralogie, Johannisallee 29, D-04103 Leipzig, Germany*
[b]*School of Chemistry, Monash University, Clayton, Melbourne, Vic 3800, Australia. E-mail: Stuart.Batten@monash.edu; Fax: +61 (03) 9905 4597; Tel: +61 (03) 9905 4606*
[c]*CSIRO Materials Science and Engineering, Private Bag 33, Clayton South MDC, Victoria, Australia. E-mail: matthew.hill@csiro.au; Fax: +61 (03) 9545 2837; Tel: +61 (03) 9545 2841*

†Electronic supplementary information (ESI) available: X-ray powder diffraction and TGA trace, Ar BET plot, Ar Isotherm and combined CO_2 plot for **1a**. CCDC 884011 (for **1a**), 884012 (for **1b**) and 884013 (for **2**). For ESI and crystallographic data in CIF or other electronic format see DOI: 10.1039/c2dt31361h

infrared (IR) spectroscopy. Furthermore, the synthetic methodology was subsequently investigated and found to be amenable to the production of gram-scale quantities of material in the case of **1a**.

Experimental details

All chemicals were obtained from Sigma-Aldrich and were used as received. Solid-state IR spectra were recorded using a Perkin Elmer 1600 series FTIR or a Bruker Equinox 55 Infrared Spectrometer fitted with a Specac Diamond ATR source. Infrared band frequencies are reported in wavenumbers (cm^{-1}) and intensities are reported as strong (s), medium (m) or weak (w). Mass spectra (MS) were recorded on a Micromass Platform II QMS spectrometer with cone voltages varying from 35 to 50 volts. Melting points were measured on a Stuart Scientific Melting Point Apparatus in an open capillary. Elemental analyses were performed by Campbell Microanalytical Laboratory, Department of Chemistry, University of Otago, Dunedin, New Zealand. Powder X-ray diffraction (XRD) measurements were performed on a Philips 1140 diffractometer with a Cu anode at λ = 1.5418 Å and a carbon monochromator. Gas adsorption isotherms for pressures in the range of 0–1.2 bar were measured by a volumetric method using a Micromeritics ASAP 2420 instrument. Freshly prepared sample was transferred to a pre-dried and weighed analysis tube which was stoppered with a Transeal cap and evacuated and activated at 50 °C under dynamic vacuum at 10^{-6} Torr for 24 h. Accurate sample masses were calculated using degassed samples. Gas adsorption measurements were performed using ultra-high purity Ar, He, H_2, CO_2 and CH_4 gas. Samples were analysed for gas adsorption capacity without exposure to air following desolvation.

The ligand **Hpma** was obtained as a crystalline solid according to a literature procedure.[12] The analytical data was consistent with prior reports. Crystalline samples of the coordination polymers, $^3_\infty$[M(**pma**)$_2$]·2X (M = Cu, **1**; Co, **2**; X = MeOH, MeCN), were obtained by either layered diffusion of a DMF solution of ligand, **Hpma** (0.10 mmol), through a buffer layer of MeOH(or MeCN)–H_2O (v/v = 1 : 1) to a methanol (or acetonitrile) solution of hydrated metal acetate (0.10 mmol), or by slow diffusion of a DMF solution of ligand, **Hpma** (0.10 mmol), into a MeCN–H_2O (v/v = 1 : 1) solution containing hydrated metal acetate (0.10 mmol).

$^3_\infty$[Cu(pma)$_2$]·2MeOH (1a)

Yield: 33 mg (77%). IR (ATR): $\tilde{\nu}$ [cm^{-1}] 3321w; 2115w; 1680w; 1639w; 1601m; 1551s; 1523s; 1503s; 1420m; 1353s; 1249m; 1214m; 1130m; 1068w; 1033w; 841m; 776s; 729s. Analyses calculated for $C_{18}H_{20}N_2O_6Cu$: C, 51.00%; H, 4.76%; N, 6.61%. Found: C, 50.94%; H, 4.72%; N, 6.59%.

$^3_\infty$[Cu(pma)$_2$]·2MeCN (1b)

Yield: 25 mg (59%). IR (ATR): $\tilde{\nu}$ [cm^{-1}] 3325w; 2250s; 1680w; 1641w; 1600m; 1552s; 1525s; 1503s; 1419m; 1351s; 1249m; 1214m; 1131m; 1065w; 1033w; 841m; 777s; 730s. Analyses calculated for $C_{20}H_{18}N_4O_4Cu$: C, 54.36%; H, 4.11%; N, 12.68%. Found: C, 54.12%; H, 4.00%; N, 12.41%.

$^3_\infty$[Co(pma)$_2$]·2MeOH (2)

Yield: 12 mg (28%). IR (ATR): $\tilde{\nu}$ [cm^{-1}] 3225w; 2115w; 1630m; 1589s; 1489m; 1421m; 1344m; 1306m; 1225w; 1001w; 933w; 839m; 825m, 691s. Analyses calculated for $C_{18}H_{20}N_2O_6Co$: C, 51.56%; H, 4.81%; N, 6.68%. Found: C, 51.42%; H, 4.77%; N, 6.57%.

Results

Characterisation of Hpma

The tautomeric nature of **Hpma** was initially investigated, resulting in the discovery of unusual solution-state properties. A symmetrical 1,3-dicarbonyl compound is expected to exhibit three conformers: the dicarbonyl, the *cis*-enolic and *trans*-enolic forms.[13] The presence of a pyridyl functionality in the α position within the acidic β-dialdehyde system eliminates the expected tautomeric forms and promotes formation of a pseudo zwitterionic species in solution, evidenced by proton NMR spectroscopy in deuterated dimethyl sulfoxide. A sharp singlet located at 9.19 ppm and integrating as two protons was assigned to the symmetrical dialdehyde groups. The resonance for the pyridinium proton, located at 5.39 ppm, was found to be severely broadened and lacking in splitting characteristics, attributed to rapid intermolecular exchange of the proton. The protonated character of the pyridine ring also results in a downfield shift of the aromatic doublets to 8.28 and 8.91 ppm. The postulated structural equilibrium of **Hpma** in solution is shown in Fig. 1. Solid-state crystallographic evidence for a *trans*-enolate zwitterionic form of **Hpma** has demonstrated the amenability of zwitterionic exchange.[14]

CP characterisation

Three coordination polymers, $^3_\infty$[M(**pma**)$_2$]·2X (M = Cu, **1a**, **1b**; Co, **2**; X = MeOH (**1a**, **2**), MeCN (**1b**)), were obtained by combining **Hpma** with hydrated metal acetates in the presence of base in either methanol or acetonitrile (Scheme 1).

Single crystals suitable for X-ray crystal structure determination were obtained by slow diffusion methods. Each of the frameworks contains a six-coordinate metal centre in a distorted octahedral conformation, ligated by six **pma** ligands. The equatorial positions are held by *trans* pyridyl and aldehyde groups. The apical positions are filled by enolato groups that offset the

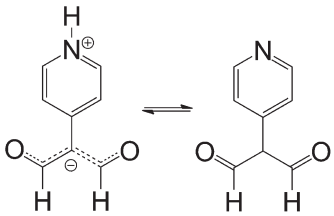

Fig. 1 Postulated rapid intermolecular exchange of **Hpma** in solution.

divalent metal cation. A summary of selected bond lengths and angles for each framework is given in Table 1. A summary of the crystal data and structural refinements for frameworks **1–2** are given in Table 2.

With exception of the identity of the lattice solvent for **1b**, framework **1a** is isostructural to both **1b** and **2**. Consequently, only the crystallographic features of **1a** will be discussed in detail. Crystallisation of **1a** occurs in the monoclinic space group $P2_1/n$ with two formula units per unit cell, which contain a copper ion coordinated by **pma** and one disordered methanol molecule. The structure of **1a**, focussing on the coordination environment of copper(II), is shown in Fig. 2. A distinct Jahn–Teller distortion is observed, with the bond length of O1d and O1e found to be significantly longer than their equatorial equivalents, O2a and O2c (2.4203(18) Å *versus* 1.9614(17) Å, respectively). This maximises separation between the two dialdehyde enolate groups in the solid-state.

Expanding the structure along each crystallographic axis reveals a three dimensional polymeric structure. The ligand **pma** may be likened to a trigonal bridge which binds three octahedral coordinated copper nodes, to generate a network with the rutile topology. In this respect, networks **1–2** can be likened to expanded variants of the Fe^{III} isonicotinato net,[15] which exhibits an identical topology, albeit with closed channels owing to the compact nature of the carboxylate group relative to the dialdinato group. The packing along the crystallographic *a*-axis using 50%

$$[M(OAc)_2]\cdot xH_2O + 2\mathbf{Hpma} \xrightarrow[-2NEt_3\cdot HOAc,\ -xH_2O]{\text{Solvent, } 2NEt_3} {}^{3}_{\infty}[M(\mathbf{pma})_2]\cdot 2\text{Solvent}$$

M = Cu, x = 1; Co, x = 4

Solvent = MeOH; MeCN

1 = (M = Cu, Solvent = MeOH)
2 = (M = Cu, Solvent = MeCN)
3 = (M = Co, Solvent = MeOH)

Scheme 1 Synthetic means of accessing coordination polymers **1–2**.

Table 1 Selected bond lengths (Å) and angles (°) for frameworks **1–2**

Framework	Bond lengths (Å)			
1a	Cu1–O1	1.9615(18)	Cu1–N1	1.983(2)
	Cu1–O2	2.4201(19)		
1b	Cu1–O1	1.9776(12)	Cu1–N1	2.0043(15)
	Cu1–O2	2.4306(13)		
2	Co1–O1	2.0695(18)	Co1–N1	1.9851(19)
	Co1–O2	2.268(2)		
	Bond angles (°)			
1a	O1–Cu1–O2	89.73(7)	O2–Cu1–N1	86.40(8)
	O1–Cu1–N1	92.25(8)		
1b	O1–Cu1–O2	90.27(5)	O2–Cu1–N1	92.58(6)
	O1–Cu1–N1	86.40(5)		
2	O1–Co1–O2	86.27(8)	O2–Co1–N1	82.95(8)
	O1–Co1–N1	87.30(8)		

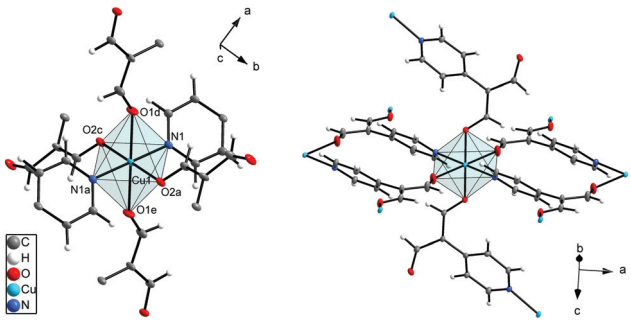

Fig. 2 Coordination environment about the copper ion of **1a**. Symmetry operators: N1a: $-x, 1-y, 1-z$; O1d: $1/2-x, y-1/2, 3/2-z$; O1e: $x-1/2, 3/2-y, z-1/2$; O2a: $1-x, 1-y, 1-z$; O2c: $x-1, y, z$. The coordination environments of **1b** and **2** are similar.

Table 2 Crystal data and structural refinements for frameworks **1–2**

Compound reference	**1a**	**1b**	**2**
Chemical formula	$C_{16}H_{12}CuN_2O_4\cdot 2(CH_4O)$	$C_{16}H_{12}CuN_2O_4\cdot 2(C_2H_3N)$	$C_{16}H_{12}CoN_2O_4\cdot 2(CH_4O)$
Formula mass	424.10	441.92	419.29
Crystal system	Monoclinic	Monoclinic	Monoclinic
a/Å	8.2220(16)	8.2896(6)	8.2010(16)
b/Å	10.509(2)	10.1177(8)	10.492(2)
c/Å	11.250(2)	11.5102(9)	11.125(2)
β/°	90.63(3)	90.944(2)	95.28(3)
Unit cell volume/Å^3	972.0(3)	965.25(13)	953.2(3)
Temperature/K	173(2)	296(2)	173(2)
Space group	$P2_1/n$	$P2_1/n$	$P2_1/n$
No. of formula units per unit cell, *Z*	2	2	2
No. of reflections measured	16 525	6074	16 040
No. of independent reflections	2443	2360	2363
No. of observed reflections	2317	1992	2241
R_{int}	0.0605	0.0308	0.0798
Final R_1 ($I > 2\sigma(I)$)	0.0475	0.0320	0.0567
Final w$R(F^2)$ ($I > 2\sigma(I)$)	0.1280	0.0783	0.1517
Final R_1 (all data)	0.0489	0.0400	0.0584
Final w$R(F^2)$ (all data)	0.1294	0.0828	0.1534
Goodness of fit on F^2	1.040	1.040	1.067

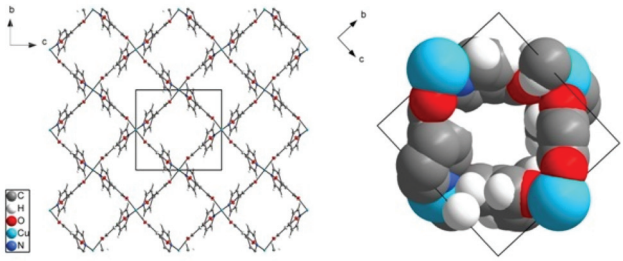

Fig. 3 Packing of **1a** along the crystallographic *a*-axis (50% probability ellipsoids, left) and space filling model of one unit cell (right). Solvent molecules have been omitted for clarity. The packing arrangement of **1b** and **2** are similar.

probability ellipsoids (left) and a space filling representation (right) are shown in Fig. 3. The coordination polymer **1** contains one dimensional pore channels along the crystallographic *a*-axis with a size of 3 × 4 Å. The theoretical pore volume calculated by PLATON[16] is 330 Å^3 and, compared to the cell volume of 971 Å^3, this value represents a theoretical porosity of 34%. The theoretical BET surface area is 567 m^2 g^{-1}. Framework **2** was found to show the greatest deviation in terms of bond lengths and unit cell dimensions relative to **1a** and **2**, which is attributed to a reduced Jahn–Teller distortion for the cobalt species ((Cu(1)–O(2): 2.4203(18) for **1a**, Cu(1)–O(2): 2.4306(13) for **1b** and Co(1)–O(2): 2.268(2) for **2**). Very little variation in the dimensions of the 1D pore channels was observed between frameworks **1**–**2**.

The synthetic methodology was next evaluated to determine the amenability for a scale-up to gram-scale quantities. Synthesis method 1 (SM1) required the mixing of equimolar solutions of **Hpma** and triethylamine (ratio 1 : 1) in dimethylformamide (DMF) with hydrated copper acetate in methanol, followed by stirring of the mixture for two hours at room temperature. Synthesis method 2 (SM2) required refluxing **Hpma** and triethylamine (ratio 1 : 1) with 1.1 equivalents of hydrated copper acetate dissolved in an equal-parts solvent mixture of water, methanol and DMF for two days. In both instances the green precipitates were isolated by filtration and air dried. The purity of the bulk powder was evaluated using X-ray powder diffraction measurements (see ESI†). The measured X-ray powder diffraction patterns were found to be in a good agreement with the simulated pattern calculated from the single crystal structure data. Minor deviations in intensity may result from variations in the identity of the guest molecules within the pore.

Thermogravimetric analysis (TGA) was next undertaken on the bulk product generated by SM2. The framework was found to undergo a weight percentage loss of 18.7%, which likely corresponds to the loss of methanol from the channels (predicted: 15.1%). A second weight percentage loss of 41.5% with an onset temperature of *ca.* 170 °C is postulated to represent liberation of pyridine as the dicarbonyl backbone of **pma** degrades (predicted: 43.4%).

Cu(**pma**)$_2$ exhibits a type I gas adsorption isotherm in measurements with Ar at 87 K, typical of a microporous material, see Fig. 4. However, the BET surface area for the material was found to be a relatively low 143 m^2 g^{-1} (see ESI†). Identical values were obtained during measurements with N_2 at

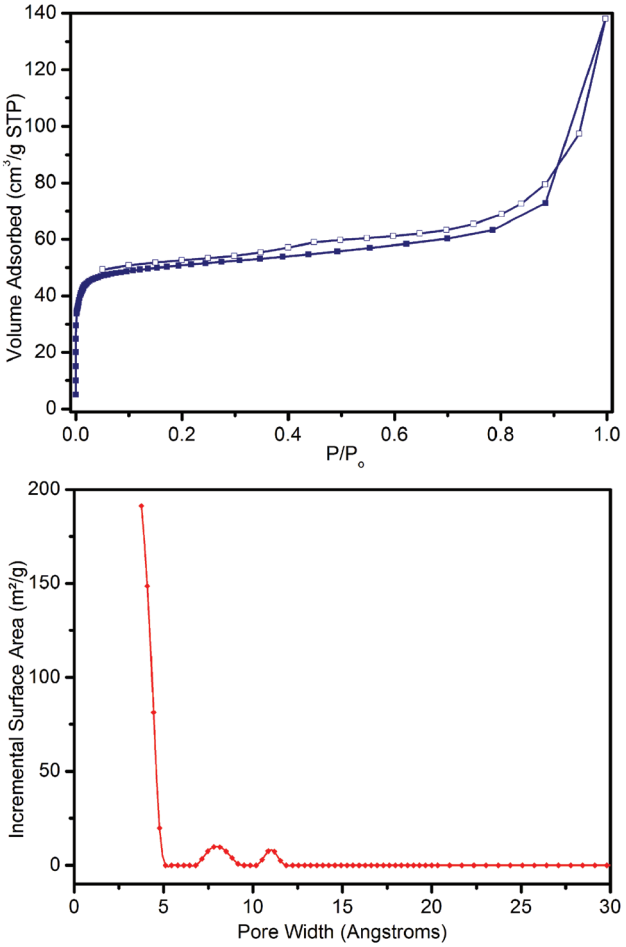

Fig. 4 Ar adsorption at 87 K for Cu(**pma**)$_2$ is typical of a microporous material (top), with the bulk of the porosity found in DFT calculations to be less than 4 Å in diameter (bottom).

77 K. Subsequent DFT pore size analyses (Fig. 4, bottom) revealed that the primary porosity in the structure following activation is below 4 Å, approaching the kinetic diameter of many gases, which is known to provide a strong adsorption strength for target gases such as carbon dioxide, hydrogen and methane. The activated material was found to be crystalline in nature as confirmed by X-ray powder diffraction analysis (see ESI†).

Fig. 5 shows gas adsorption analyses performed at 273 K for nitrogen, carbon dioxide and methane, along with hydrogen adsorption at 77 K. Relative to the low surface area, uptake of hydrogen and carbon dioxide in particular is significant, being 0.54 and 13.8 wt% respectively. Cu(**pma**)$_2$ shows adsorption selectivity for carbon dioxide over methane and nitrogen, areas of particular interest for natural gas sweetening and post combustion capture. Whilst the selectivities are not high enough to be regarded as industrially relevant, it is notable that the CO_2 adsorption capacity is in excess of that employed in commercial post-combustion capture amine adsorbents, which can absorb around 11 wt%.[17] This demonstrates the utility of porous adsorbents for CO_2 capture, and underlines the strong affinity for CO_2 witnessed for a material of such low BET surface area. Fig. 6 puts the exceptional relative adsorption for CO_2 into perspective. A plot of surface area *versus* volumetric uptake at 273 K reveals

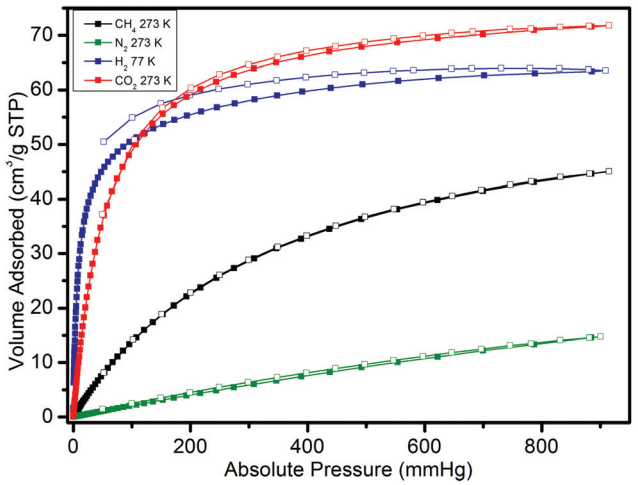

Fig. 5 The strong adsorption capacities of Cu(**pma**)$_2$ relative to its surface area.

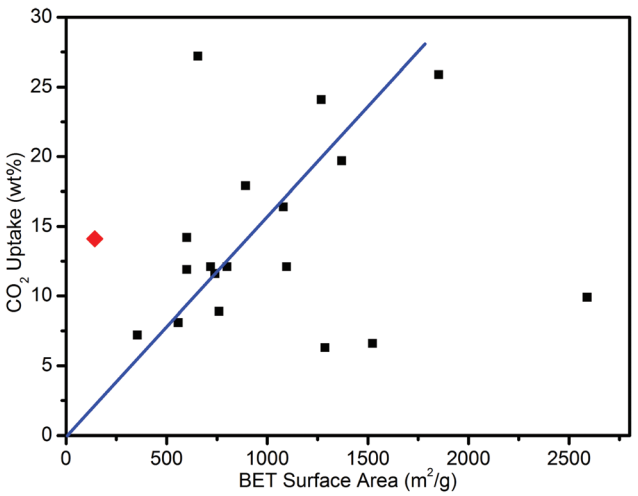

Fig. 6 Cu(**pma**)$_2$ adsorbs very large quantities of CO_2 relative to its low surface area. Data adapted from Sumida *et al.*[18]

a broad relationship between surface area and storage capacity for reported frameworks, for which Cu(**pma**)$_2$ sits well above. Clearly the channel size and surface chemistry are well suited to CO_2 adsorption.

Indeed the affinity for CO_2 is confirmed in Fig. 7. A plot of adsorption enthalpy *versus* adsorption coverage, calculated by virial methods[18] shows a consistently high value around 40 kJ mol^{-1}, which is one of the higher values reported in CPs for CO_2 adsorption,[18] and is all the more significant due to the lack of drop-off with increased coverage, something typically witnessed in materials where there are a limited number of attractive adsorptive sites. In this case the size of the channel delivers strong adsorption for all loading levels. Enthalpy of adsorption for hydrogen is close to the typical values observed for Cu-containing frameworks;[1] the lack of increase here accounted for by the channels being better suited to the slightly larger carbon dioxide.

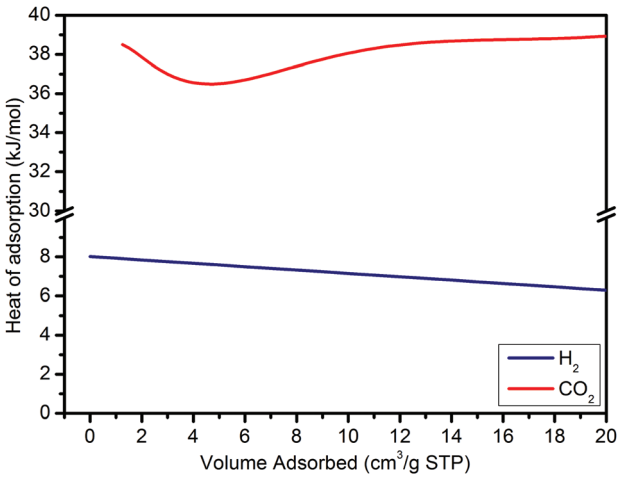

Fig. 7 The large relative CO_2 capacity is reflected in a strong adsorption enthalpy irrespective of loading level. The strong hydrogen adsorption enthalpy is typical of a material with exceptionally small pores.

Conclusions

A new family of microporous CPs has been identified and characterised. Cu(**pma**)$_2$ exhibited a typical type I gas adsorption isotherm and, despite a relatively low total surface area, a large carbon dioxide adsorption value was observed. This is likely due to the high affinity carbon dioxide exhibits towards the surface chemistry and pore dimensions of the CP, reflected by a calculated adsorption enthalpy value of 38 kJ mol^{-1}.

Acknowledgements

This research is supported by the Science and Industry Endowment Fund, the Australian Research Council, and Monash University. Universität Leipzig is thanked for allowing P. E. to participate in the ISAP exchange program. This research was, in part, undertaken on the macromolecular crystallography (MX1) beamline at the Australian Synchrotron, Victoria, Australia.

Notes and references

1 L. J. Murray, M. Dincă and J. R. Long, *Chem. Soc. Rev.*, 2009, **38**, 1294; A. W. C. van den Berg and C. Otero Areán, *Chem. Commun.*, 2008, 668; G. J. Kubas, *Metal Dihydrogen and σ-Bond Complexes – Structure, Theory and Reactivity*, Kluwer Academic, New York, Boston, Dordrecht, London, Moscow, 2001; C. H. Wu, *J. Chem. Phys.*, 1979, **71**, 783; M. Dincă and J. R. Long, *Angew. Chem., Int. Ed.*, 2008, **47**, 6766; S. S. Kaye and J. R. Long, *J. Am. Chem. Soc.*, 2008, **130**, 806; K. L. Mulfort and J. T. Hupp, *J. Am. Chem. Soc.*, 2007, **129**, 9604.

2 S. Q. Ma, D. F. Sun, J. M. Simmons, C. D. Collier, D. Q. Yuan and H. C. Zhou, *J. Am. Chem. Soc.*, 2008, **130**, 1012.

3 S. R. Batten, S. M. Neville and D. R. Turner, *Coordination Polymers: Design, Analysis and Application*, Royal Society of Chemistry, Thomas Graham House, Science Park, Milton Road, Cambridge CB4 0WF, UK, 2008; M. Eddaoudi, J. Kim, N. Rosi, D. Vodak, J. Wachter, M. O'Keeffe and O. M. Yaghi, *Science*, 2002, **295**, 469; S. Kitagawa, R. Kitaura and S. Noro, *Angew. Chem., Int. Ed.*, 2004, **43**, 2334; S. R. Batten and R. Robson, *Angew. Chem., Int. Ed.*, 1998, **37**, 1460; M. Eddaoudi, D. B. Moler, H. L. Li, B. L. Chen, T. M. Reineke, M. O'Keeffe and O. M. Yaghi, *Acc. Chem. Res.*, 2001, **34**, 319; O. M. Yaghi, M. O'Keeffe, N. W. Ockwig, H. K. Chae, M. Eddaoudi and J. Kim, *Nature*, 2003, **423**, 705; A. K. Cheetham, G. Ferey and T. Loiseau,

Angew. Chem., Int. Ed., 1999, **38**, 3268; O. M. Yaghi, H. L. Li, C. Davis, D. Richardson and T. L. Groy, *Acc. Chem. Res.*, 1998, **31**, 474.
4 Multi-Year Research, Development and Demonstration Plan – Planned Program Activities for 2003–2010, Technical Plan, U.S. Department of Energy, http://www.eere.energy.gov/hydrogenandfuelcells/mypp/pdfs/storage.pdf; A. Celzard and V. Fierro, *Energy Fuels*, 2005, **19**, 573.
5 K. Sumida, M. R. Hill, S. Horike, A. Dailly and J. R. Long, *J. Am. Chem. Soc.*, 2009, **131**, 15120; A. W. Thornton, K. M. Nairn, J. M. Hill, A. J. Hill and M. R. Hill, *J. Am. Chem. Soc.*, 2009, **131**, 10662.
6 B. Chem, F. R. Fronczek and A. W. Maverick, *Chem. Commun.*, 2003, 2166; S. S. Turner, D. Collison, F. E. Mabbs and M. Halliwell, *J. Chem. Soc., Dalton Trans.*, 1997, 1117.
7 V. D. Vreshch, A. N. Chernega, J. A. K. Howard, J. Sieler and K. V. Domasevitch, *Dalton Trans.*, 2003, 1707.
8 V. D. Vreshch, A. B. Lynko, A. N. Chernega, J. A. K. Howard, H. Krautscheid, J. Sieler and K. V. Domasevitch, *Dalton Trans.*, 2004, 2899.
9 K. V. Domasevitch, *Acta Crystallogr., Sect. C*, 2008, **64**, m105.
10 C. Reichardt, *Solvents and Solvent Effects in Organic Chemistry*, 3rd edn, Wiley-VCH, 2003, p. 106; R. S. Noy, V. A. Gindin and B. A. Ershov, *Org. Magn. Reson.*, 1975, **7**, 109; R. Matusch, *Angew. Chem., Int. Ed. Engl.*, 1975, **4**, 260.
11 C. A. Tovee, C. A. Kilner, J. A. Thomas and M. A. Halcrow, *CrystEngComm*, 2007, **9**, 361.
12 Y. Mulyana, C. J. Kepert, L. F. Lindoy, A. Parkin and P. Turner, *Dalton Trans.*, 2005, 1598.
13 C. Reichardt, *Solvents and Solvent Effects in Organic Chemistry*, 3rd edn, Wiley-VCH, 2003, 106; R. S. Noy, V. A. Gindin and B. A. Ershov, *Org. Magn. Reson.*, 1975, **7**, 109; R. Matusch, *Angew. Chem., Int. Ed. Engl.*, 1975, **4**, 260.
14 C. A. Tovee, C. A. Kilner, J. A. Thomas and M. A. Halcrow, *CrystEngComm*, 2007, **9**, 361.
15 R.-G. Xiong, S. R. Wilson and W. Lin, *J. Chem. Soc., Dalton Trans.*, 1998, 4089.
16 A. L. Speck, *PLATON, a Multipurpose Crystallographic Tool*, Utrecht University, Utrecht, The Netherlands, 2001, http://www.cryst.chem.uu.nl/platon/
17 A. J. Reynolds, T. V. Verheyen, S. B. Adeloju, E. Meuleman and P. Feron, *Environ. Sci. Technol.*, 2012, **46**, 3643–3654; A. Cousins, L. T. Wardhaugh and P. H. M. Feron, *Int. J. Greenhouse Gas Control*, 2011, **5**, 605–619; M. R. M. Abu-Zahra, J. P. M. Niederer, P. H. M. Feron and G. F. Versteeg, *Int. J. Greenhouse Gas Control*, 2007, **1**, 135–142.
18 K. Sumida, D. L. Rogow, J. A. Mason, T. M. McDonald, E. D. Bloch, Z. R. Herm, T.-H. Bae and J. R. Long, *Chem. Rev.*, 2012, **112**, 724–781.